The Astrophysical Journal Letters, 733:L34 (5pp), 2011 June 1 doi:10.1088/2041-8205/733/2/L34

DETECTION OF CURRENT SHEETS AND MAGNETIC RECONNECTIONS AT THE TURBULENT LEADING EDGE OF AN INTERPLANETARY CORONAL MASS EJECTION

Abraham C.-L. Chian[1,2] and Pablo R. Muñoz[2]
[1] California Institute of Technology, Pasadena, CA 91125, USA
[2] National Institute for Space Research (INPE) and World Institute for Space Environment Research (WISER), P.O. Box 515, São José dos Campos SP 12227-010, Brazil; abraham.chian@gmail.com, pablocus@gmail.com
Received 2010 November 25; accepted 2011 April 18; published 2011 May 10

ABSTRACT

The relation between current sheets, turbulence, and magnetic reconnections at the leading edge of an interplanetary coronal mass ejection detected by four *Cluster* spacecraft on 2005 January 21 is studied. We report the observational evidence of two magnetically reconnected current sheets in the vicinity of a front magnetic cloud boundary layer with the following characteristics: (1) a Kolmogorov power spectrum in the inertial subrange of the magnetic turbulence, (2) the scaling exponent of structure functions of magnetic fluctuations exhibiting multi-fractal scaling predicted by the She–Leveque magnetohydrodynamic model, and (3) bifurcated current sheets with the current density computed by both single-spacecraft and multi-spacecraft techniques.

Key words: magnetic reconnection – plasmas – shock waves – solar wind – Sun: coronal mass ejections (CMEs) – turbulence

Online-only material: color figures

1. INTRODUCTION

Identification of coherent structures is a key to probing the nature of intermittent turbulence in astrophysical plasmas such as the solar wind (Bruno & Carbone 2005; Borovsky 2010). Current sheets are magnetic coherent structures in a localized region of electric current confined to a nearly two-dimensional surface, ubiquitous in a magnetized astrophysical plasma (Veltri 1999), which have been seen in numerical simulations (Zhou et al. 2004), solar wind (Gosling et al. 2005, 2007; Phan et al. 2006; Li 2008), and solar flares (Liu et al. 2010). Magnetic reconnection in a current sheet is a fundamental mechanism that converts magnetic energy into plasma kinetic energy in astrophysical systems (Nishida 2007; Priest 2007). An interplanetary shock and magnetic cloud boundary layer (MCBL) are formed by the interaction of an interplanetary coronal mass ejection (ICME) emanating from a solar active region with the ambient solar wind (Wei et al. 2003a, 2003b; Bougeret & Pick 2007; Cargill & Harra 2007), which lead to a local enhancement of intermittency in the interplanetary turbulence, characterized by the kurtosis–skewness interdependence, via cross-scale coupling between large-scale structures such as shock boundaries and small-scale fluctuations (Vörös et al. 2006).

In this Letter, we study the relation between current sheets, turbulence, and magnetic reconnections at the leading edge of an ICME intercepted by the four *Cluster* spacecraft in the solar wind on 2005 January 21 (Foullon et al. 2007; Du et al. 2008; Miranda et al. 2010; Muñoz et al. 2010). A few papers that deal with magnetic turbulence in ICME only tackle the region inside a magnetic cloud (Leamon et al. 1998; Liu et al. 2006). We report for the first time the observational evidence of a Kolmogorov magnetic turbulence in the vicinity of two magnetically reconnected current sheets at the front MCBL that exhibits the She–Leveque multi-fractal scaling and signatures of bifurcated current sheets. Recent investigations of interplanetary and geomagnetic data show that the leading edge of an ICME triggers the initial phase of geomagnetic storms (Du et al. 2008; Zuo et al. 2010). Hence, an improved knowledge of the physical processes that occur at/near the front MCBL is important for understanding the dynamics of star–planet relation.

2. OBSERVATIONS AND DISCUSSIONS

Figure 1(a) provides an overview of the modulus of magnetic field $|\mathbf{B}|$ measured by *Cluster-1* from 16:51:00 UT to 19:30:00 UT on 2005 January 21, when the four *Cluster* spacecraft are located upstream of Earth's bow shock. The primary bow shock (SA) at 17:10:20 UT indicates a sudden jump of $|\mathbf{B}|$ from ∼5 nT to ∼30 nT, accompanied by jumps in the modulus of ion velocity $|\mathbf{V}|$, ion density N_i, ion temperature T_i, and plasma β (Foullon et al. 2007; Muñoz et al. 2010). The leading edge of ICME (SB) at 18:44:11 UT marks the starting point of a non-compressive density enhancement region where N_i increases abruptly from ∼13 cm^{-3} to ∼40 cm^{-3}, which is followed by a magnetic cloud. SB is associated with an increase of β. The boundaries of this ejecta front layer are formed by two magnetic coherent structures SB1 and SB2 (Foullon et al. 2007; Muñoz et al. 2010). An enlargement of the vicinity of the leading edge of ICME, given by the time interval from 18:32:30 UT to 18:56:51 UT, is shown in Figure 1(b). This interval contains $2^{15} = 32{,}768$ data points.

A technique to identify current sheets in the solar wind using a single-spacecraft magnetic field measurement was introduced by Li (2008). According to this technique, in order to determine the presence of current sheets in a given time interval of $\mathbf{B}(t)$ it is necessary to prove first that an integrated distribution function $F(\theta, T)$ for the time interval, representing the probability of finding the angle between $\mathbf{B}(t)$ and $\mathbf{B}(t+T)$ larger than θ, scales linearly with the time lag T when the angle θ is larger than a critical angle θ_0, namely, $F(\theta, NT) \sim NF(\theta, T)$, where N is an arbitrary integer greater than zero. By applying this technique to the magnetometer data of *Cluster-1* for the time interval of Figure 1(a), and assuring that a linear behavior is seen in a range of timescales (T from 30 s to 240 s) and a range of angles (θ from 60° to 120°), we find a large number of current sheets (magenta dots) in the sheath region of ICME as demonstrated in

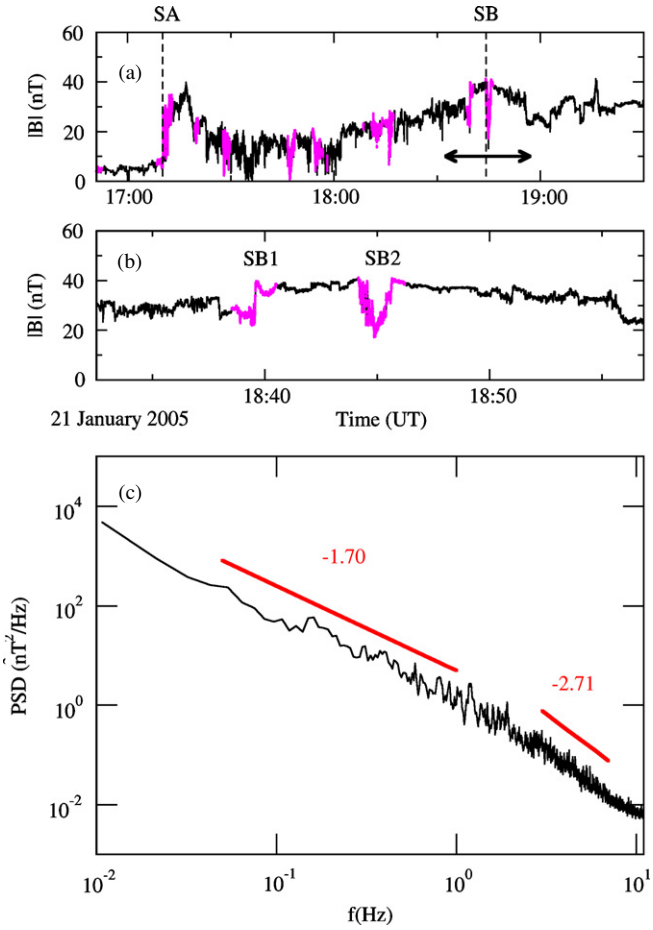

Figure 1. Detection of current sheets and magnetic turbulence by *Cluster-1* at the ICME shock of 2005 January 21. (a) Time series of |**B**| (nT) superposed by current sheets detected by the Li (2008) method, for the critical angle $\theta = 60^\circ$ and the timescale $T = 120$ s. Magenta dots indicate the points that belong to a current sheet. SA denotes the primary shock arrival. SB1 and SB2 denote the two current sheets associated with the leading edge (SB) of the ICME ejecta. (b) An enlargement of the time interval marked by a bar in (a). (c) Power spectral density, PSD (nT^2 Hz^{-1}), of |**B**| for the time interval of (b); straight lines indicate the inertial and dissipative subranges. The spectral indices are calculated by a linear regression of the log–log PSD data.

(A color version of this figure is available in the online journal.)

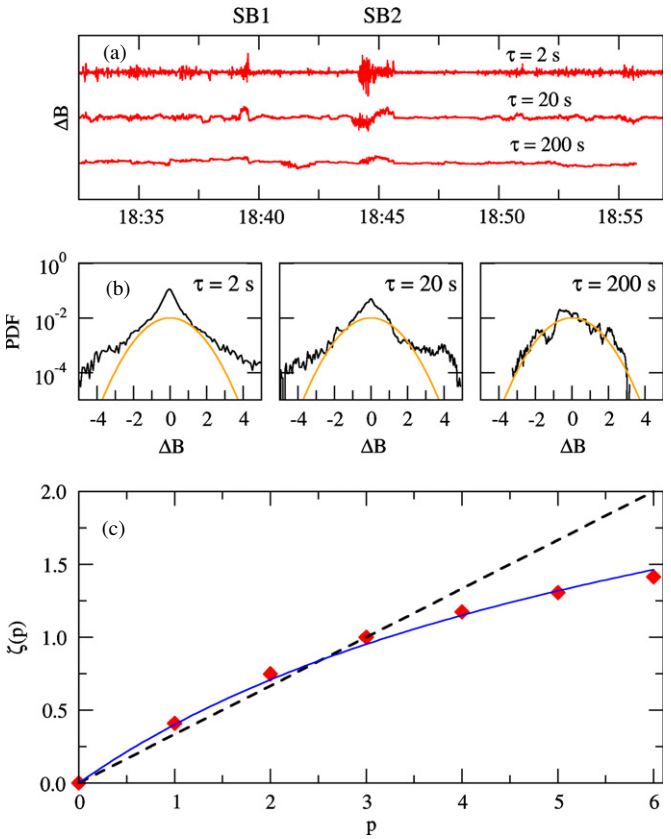

Figure 2. Scale dependence for three different timescales ($\tau = 2$ s, 20 s, and 200 s) of Figure 1(b). (a) The normalized magnetic-field two-point differences ΔB. (b) The probability density function (PDF) of ΔB, superposed by a Gaussian PDF (orange line). (c) Scaling exponent ζ of the pth-order structure function for observed values (red diamonds), superposed by the K41 self-similar scaling (black dashed line), and the multi-fractal prediction of the She–Leveque MHD model (blue curve).

(A color version of this figure is available in the online journal.)

Figure 1(a). Our results show that the technique of Li (2008) is capable of detecting current sheets of any scale $T \gg \delta$, where δ is the temporal resolution of data. In particular, we identify two current sheets SB1 and SB2 at the leading edge of ICME, which form behind a magnetic discontinuity as seen in Figure 1(b). The interplanetary magnetic field (IMF) points toward the Sun ($B_x > 0$) and southward ($B_z < 0$), in the Geocentric Solar Ecliptic (GSE) coordinates, before and after the passage of the ejecta front layer. Within the front layer itself, between SB1 and SB2, the IMF points almost in the opposite direction (away from the Sun $B_x < 0$ and northward $B_z > 0$), whereas B_y turns smoothly from negative to positive (Foullon et al. 2007). **B** has a strong shear angle ($\theta_{SB1} \sim 146^\circ$ and $\theta_{SB2} \sim 150^\circ$) between the leading and trailing boundaries of SB1 and SB2.

The power spectral density (PSD) in Figure 1(c) of the time series of magnetic fluctuations of Figure 1(b) is computed using the Welch method (Welch 1967), by dividing the time series into a set of overlapping subintervals and computing the PSD of each subinterval by the fast Fourier transform. The average of the set of power spectra gives the PSD of Figure 1(c). The spectral index for the inertial subrange -1.70 ± 0.05 is calculated by a linear regression of the log–log PSD data in the frequency range 0.05–1 Hz, which is determined by the compensated PSD technique of Biskamp et al. (1999). The same procedure is applied to obtain the spectral index for the dissipative subrange -2.71 ± 0.05 in the frequency range 3–7 Hz. The correlation coefficients r^2 of the linear regression are 0.93 and 0.86, respectively, for the inertial and dissipative subranges. Figure 1(c) provides the first observational evidence of a Kolmogorov power spectra $-5/3$ in the inertial subrange of the magnetic turbulence in the vicinity of a front MCBL.

The scale dependence for three different timescales ($\tau =$ 2 s, 20 s, 200 s) of the normalized two-point difference of the modulus of magnetic field and the probability density function (PDF) are shown in Figures 2(a) and 2(b), where $\Delta B = (\delta B - \langle \delta B \rangle)/\sigma_B$, $\delta B(\tau) = |\mathbf{B}(t+\tau)| - |\mathbf{B}(t)|$ denotes the two-point difference of |**B**| for a given timescale τ, the angle brackets denote the mean value of δB, and σ_B denotes the standard deviation of δB. Figure 2(a) shows that the magnetic field fluctuations at the leading boundary of the ICME, in the vicinity of the two current sheets SB1 and SB2, become more intermittent as the scale becomes smaller. The three timescales in Figure 2(a) correspond to 1858 km, 18,580 km, and 185,800 km, respectively, if we assume the Taylor's hypothesis and use the mean ion bulk speed of $\langle |\mathbf{V}_{SW}| \rangle = 929$ km s^{-1} measured in this time interval. Figure 2(b) shows that the PDF of ΔB at

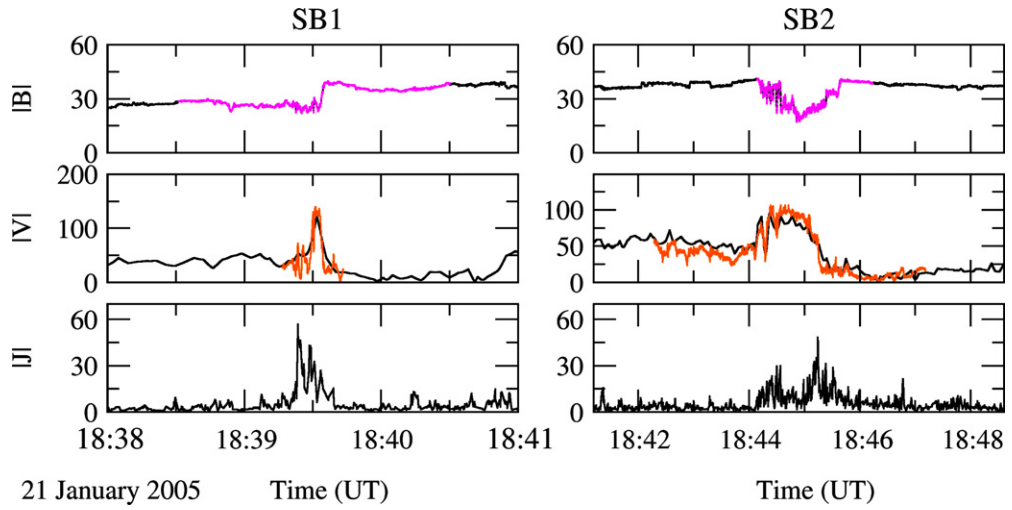

Figure 3. Detection of magnetic reconnections at the leading edge of ICME associated with the current sheets SB1 and SB2 (magenta). $|\mathbf{B}|$ (nT) is the modulus of magnetic field (enlargement of Figure 1(b)); $|\mathbf{V}|$ (km s^{-1}) is the modulus of the observed plasma velocity (black) and the plasma velocity (orange) predicted by the magnetic reconnection theory of Sonnerup et al. (1981); $|\mathbf{J}|$ (nA m^{-2}) is the modulus of current density computed by the multi-spacecraft curlometer technique of Dunlop et al. (2002).

(A color version of this figure is available in the online journal.)

the leading edge of the ICME is close to a Gaussian distribution at large timescales, but deviates significantly from a Gaussian distribution as the timescale decreases. At small scales, the shape of the PDF becomes non-Gaussian and leptokurtic, displaying sharp peaks at $\Delta B \sim 0$ and fat tails at large ΔB, due to an excess of small- and large-amplitude fluctuations in the SB1 and SB2 regions seen in Figure 2(a).

We characterize first the multi-fractal nature of the turbulent boundary layers at the leading edge of ICME by comparing the scaling exponents of structure functions of magnetic fluctuations, $S_p(\tau) = \langle|\delta B(\tau)|^p\rangle \sim \tau^{\alpha(p)}$ (where the angle brackets denote ensemble averaging over time, and p denotes the order of structure functions), within the inertial subrange against Kolmogorov's K41 universality theory which is based on the simplified assumptions of homogeneity, isotropy, incompressibility, and stationarity (Politano & Pouquet 1995). The scaling exponent for each integer order p of the structure function can be obtained by estimating the slope of a linear fitting of the curves within the inertial subrange. We then apply the extended self-similarity (ESS) technique of Benzi et al. (1993) to improve the calculation of the scaling exponent, $S_p(\tau) \sim [S_3(\tau)]^{\zeta(p)}$, where $\zeta(p) \sim \alpha(p)/\alpha(3)$ is found from the extended range. Figure 2(c) shows the scaling exponent $\zeta(p)$ as a function of p for the time series of Figure 1(b). The black dashed line denotes the K41 self-similar scaling, $\zeta(p) = p/3$. The statistical scaling properties of the observed magnetic fluctuations (indicated by a diamond symbol) in Figure 2(c) display a noticeable departure from self-similarity. As shown by Figures 2(a) and 2(b), the origin of intermittency and non-Gaussianity is the excess of small-scale, large-amplitude fluctuations in the regions of SB1 and SB2. The coherent structures such as SB1 and SB2 embedded in the intermittent magnetic turbulence result from amplitude–phase synchronization related to nonlinear multi-scale interactions (Koga et al. 2007; Chian & Miranda 2009; Chian et al. 2010b).

Several models have been proposed to improve the prediction of universality in fluid and magnetohydrodynamic (MHD) turbulence. A model of universal scaling laws for fully developed turbulence in fluids was postulated by She & Leveque (1994) in terms of scaling of a sequence of moment ratios of the energy dissipation field coarse grained at the inertial subrange scale, whereby the moment ratios form a hierarchy of structures and the most singular structures are assumed to be vortex filaments. This model is successful in reproducing both experimental and numerical data of fluid and plasma turbulence. An extension of the universal scaling of She & Leveque (1994) was developed by Politano & Pouquet (1995) in the framework of the Iroshnikov–Kraichnan theory of MHD turbulence for sheetlike dissipative structures, and by Müller & Biskamp (2000) and Müller et al. (2003) within the framework of the Kolmogorov $k^{-5/3}$ law for sheetlike dissipative structures in isotropic and anisotropic MHD turbulence, respectively. In Figure 2(c) we compare the observed scaling exponents of magnetic turbulence with the She–Leveque MHD model (blue curve) of Müller et al. (2003), $\zeta_p = p/g^2 + 1 - (1/g)^{p/g}$, where g is an adjustable parameter. Evidently, the prediction of the She–Leveque model for anisotropic MHD turbulence closely reproduces the observed scaling of interplanetary magnetic turbulence, for $g = 3.2257$. Our results also render support for the anisotropic Kolmogorov theory of Alfvén turbulence developed by Goldreich & Sridhar (1995) and present the first evidence of the multi-fractal universality of magnetic fluctuations in the neighborhood of a front MCBL.

We discuss next the detection of magnetic reconnections associated with the two currents sheets SB1 and SB2. Figure 3 shows the time series of the modulus of magnetic field $|\mathbf{B}|$ (nT), the modulus of observed ion velocity $|\mathbf{V}|$ (km s^{-1}, black line) and the plasma velocity (orange line) predicted by the magnetic reconnection theory of Sonnerup et al. (1981), and the modulus of current density $|\mathbf{J}|$ (nA m^{-2}) computed from $\mathbf{B}$ by the curlometer method of Dunlop et al. (2002) using four *Cluster* spacecraft. Intense localized current density is clearly seen in the regions of SB1 and SB2 in Figure 3. The magnetic field data of SB1 and SB2 is analyzed using the minimum variance analysis (MVA) to find the direction along which the field component has minimum variance (N direction), and the directions of maximum (L) and intermediate (M) variance (Sonnerup & Cahill 1967). These three directions form an orthogonal LMN coordinate system (see Figure 1 of Phan et al. 2006). Considering a current sheet as a two-dimensional planar magnetic structure

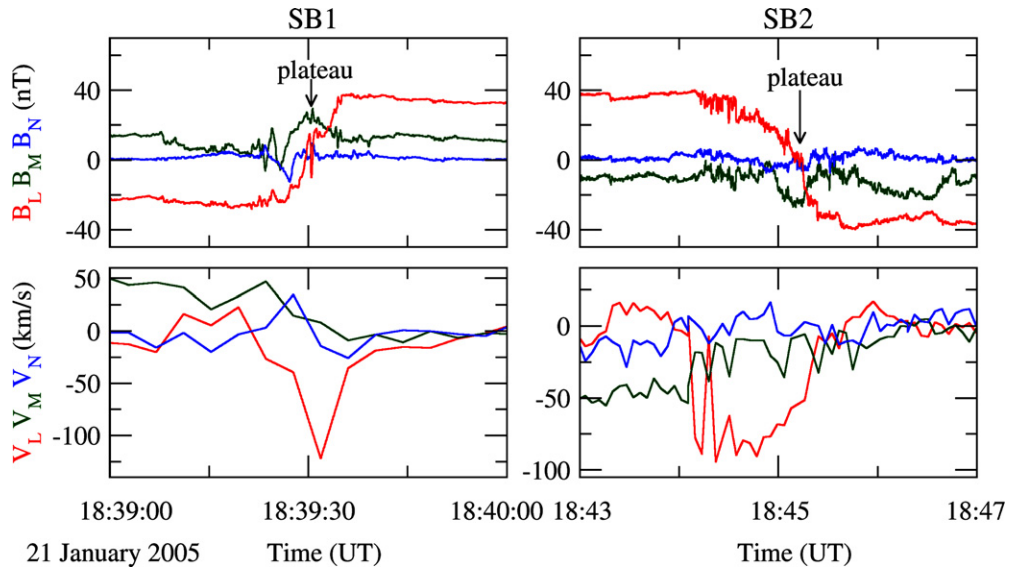

Figure 4. B_L (red), B_M (green), and B_N (blue) are the components of **B** measured by *Cluster-1* in the LMN coordinates; V_L (red), V_M (green), and V_N (blue) are the components of **V**. This figure shows observational evidence of bifurcated current sheets SB1 and SB2, with a plateau at B_L in the middle of each bifurcated current sheet, and counter-propagating Alfvén waves at two edges of SB1 and SB2.

(A color version of this figure is available in the online journal.)

formed by two sets of oppositely directed field lines lying in a plane, L is then the direction of the field lines, M is the out-of-plane direction, and N is the direction perpendicular to L and M. A thin current sheet is formed between the two oppositely directed field lines, with the current flowing in the M direction. When the oppositely directed field lines reconnect, the current sheet bifurcates. Figure 4 shows three components of magnetic field (B_L, B_M, B_N) and ion velocity (V_L, V_M, V_N) in the LMN coordinates. For visualization we have shifted the plasma velocities in Figures 3 and 4 by the average solar wind velocity, given by $\langle \mathbf{V}_{SW} \rangle = (-926, 75, -29)$ km s^{-1} in the GSE coordinates.

A signature of a bifurcated current sheet is the appearance of a "plateau" in B_L in the middle of a current sheet related to the region of the reconnection jet, as well as counter-propagating Alfvén waves evidenced by correlated/anti-correlated B_L and V_L at two edges of a current sheet (Gosling et al. 2005, 2007; Phan et al. 2006). This signature is readily seen in Figures 3 and 4 for both SB1 and SB2. Each current sheet SB1 and SB2 is associated with a respective strong jet of ion flow $|\mathbf{V}|$ shown in the middle panels of Figure 3, which flows mainly in the L direction as seen in the lower panels of Figure 4, in agreement with the geometry of a magnetically reconnected current sheet. The observed jet velocity is close to the velocity predicted by the magnetic reconnection theory of Sonnerup et al. (1981), shown in the middle panels of Figure 3. Figure 4 shows that V_L is anti-correlated (correlated) with B_L at the leading (trailing) boundary of the current sheet SB1, and V_L is correlated (anti-correlated) with B_L at the leading (trailing) boundary of the current sheet SB2. Such pairs of oppositely coupled changes in **V** and **B** are the signatures of counter-propagating Alfvén waves and provide observational support for magnetic reconnection exhausts in bifurcated current sheets in the solar wind (Gosling et al. 2005, 2007; Phan et al. 2006).

To clarify further the signature of a bifurcated current sheet, we plot in Figure 5 B_L measured by *Cluster-3*, and J_M estimated from B_L near the plateau of SB1. By assuming time stationarity and planarity of the current sheet, we compute J_M from a single

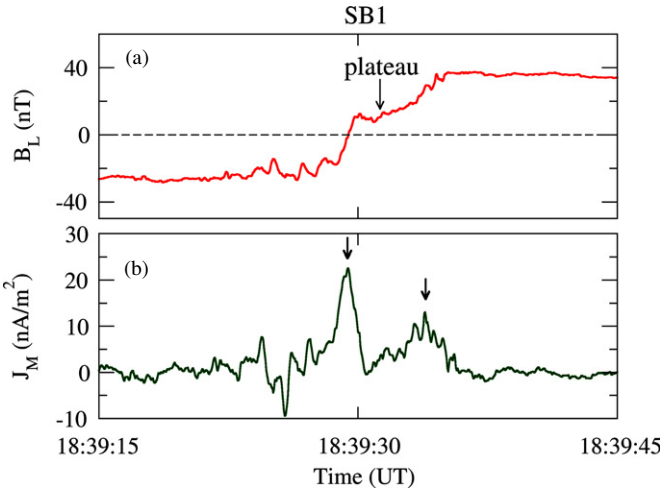

Figure 5. Direct evidence of a bifurcated current sheet SB1 measured by *Cluster-3*. (a) Two-step temporal variation of B_L with a plateau in the middle of the current sheet. (b) J_M calculated from B_L showing double peaks at both edges of the current sheet.

(A color version of this figure is available in the online journal.)

spacecraft by the Ampere's Law, $J_M = (\Delta B_L/\Delta t)/(\mu_0 V_{CS})$, where the spatial derivative is substituted by the temporal derivative using the Taylor's hypothesis and V_{CS} is the normal speed of the current sheet (Mozer et al. 2008). Figure 5(a) shows that the temporal variation of the reconnected component of magnetic field B_L occurs in two main steps which is evidence that SB1 is bifurcated. Moreover, Figure 5(b) shows two peaks (indicated by arrows) in the out-of-plane component of current density J_M, at two edges of SB1, demonstrating that the current sheet is bifurcated. Such direct evidence of a double-peak bifurcated current sheet has been previously obtained in association with magnetic reconnections in the Earth's magnetotail (Hoshino et al. 1996) and in the magnetosheath of Earth's bow shock (Retinò et al. 2007). This is the first time such an observation is demonstrated in an ICME.

3. CONCLUSION

Current sheets and magnetic reconnections play a fundamental role in many regions of the heliosphere (Kamide & Chian 2007, p. 10; Paschmann 2008). A statistical analysis of boundary layers of a large number of magnetic clouds indicated that MCBLs are formed by the interaction between magnetic clouds and the ambient solar wind, which may be linked to the outer loops of an ICME and often display the properties of magnetic reconnection (Wei et al. 2003b), as confirmed by numerical simulations (Schmidt & Cargill 2003) and models (Dasso et al. 2006) of the magnetic-cloud–solar-wind interaction. In fact, magnetic reconnection exhausts have been observed at the front and rear edges of a number of ICMEs (Gosling et al. 2005, 2007). Hence, our study of the relation between currents sheets, turbulence, and magnetic reconnection in the neighborhood of a front MCBL is key to understand the dynamics and structure of ICME boundary layers, and can aid in forecasting the onset of a geomagnetic storm caused by an ICME (Du et al. 2008; Zuo et al. 2010).

We characterized for the first time the multi-fractal nature of a Kolmogorov magnetic turbulence at the leading edge of an ICME where two bifurcated current sheets with signatures of magnetic reconnections are found. Our methodology can be readily applied to other turbulent boundary layers of astrophysical plasmas, such as termination and bow shocks of the heliosphere and astrospheres (Stone et al. 2008; Sahai & Chronopoulos 2010). Further studies of the magnetic-cloud–solar-wind coupling will improve our understanding of the dynamics of star–planet relation and search for exoplanets (Kivelson 2007; Chian et al. 2010a).

The authors thank S. Dasso, E. Echer, G. Li, R. Miranda, A. Retinò, and B. Tsurutani for valuable discussions, and the *Cluster* FGM and CIS instrument teams for open access to their data. This research is supported by CAPES and CNPq. A.C.L.C. acknowledges the award of a Guggenheim Fellowship and the hospitality of Caltech. P.R.M. acknowledges the award of a Roberto Manzano Prize for the Best Student Paper of IX COLAGE.

REFERENCES

Benzi, R., Ciliberto, S., Tripiccione, R., Baudet, C., Massaioli, F., & Succi, S. 1993, Phys. Rev. E, 48, 29
Biskamp, D., Schwartz, E., Zeiler, A., Celani, A., & Drake, J. F. 1999, Phys. Plasmas, 6, 751
Borovsky, J. E. 2010, Phys. Rev. Lett., 105, 111102
Bougeret, J.-L., & Pick, M. 2007, in Handbook of the Solar–Terrestrial Environment, ed. Y. Kamide & A. C.-L. Chian (Berlin: Springer), 134
Bruno, R., & Carbone, V. 2005, Living Rev. Sol. Phys., 2, 4
Cargill, P. J., & Harra, L. K. 2007, in Handbook of the Solar–Terrestrial Environment, ed. Y. Kamide & A. C.-L. Chian (Berlin: Springer), 118
Chian, A. C.-L., & Miranda, R. A. 2009, Ann. Geophys., 27, 1789
Chian, A. C.-L., Han, M., Miranda, R. A., Shu, C., & Valdivia, J. A. 2010a, Adv. Space Res., 46, 472
Chian, A. C.-L., Miranda, R. A., Rempel, E. L., Saiki, Y., & Yamada, M. 2010b, Phys. Rev. Lett., 104, 254102
Dasso, S., Mandrini, C. H., Démoulin, P., & Luoni, M. L. 2006, A&A, 455, 349
Du, A. M., Tsurutani, B. T., & Sun, W. 2008, J. Geophys. Res., 113, A10214
Dunlop, M. W., Balogh, A., Glassmeier, K.-H., & Robert, P. 2002, J. Geophys. Res., 107, A1384
Foullon, C., et al. 2007, Sol. Phys., 244, 139
Goldreich, P., & Sridhar, S. 1995, ApJ, 438, 763
Gosling, J. T., Eriksson, S., McComas, D. J., Phan, T. D., & Skoug, R. M. 2007, J. Geophys. Res., 112, A08106
Gosling, J. T., Skoug, R. M., McComas, D. J., & Smith, C. W. 2005, J. Geophys. Res., 110, A01107
Hoshino, M., Nishida, A., Mukai, T., Saito, Y., Yamamoto, T., & Kokubun, S. 1996, J. Geophys. Res., 101, A24775
Kamide, Y., & Chian, A. C.-L. (ed.) 2007, Handbook of the Solar–Terrestrial Environment (Berlin: Springer), 10
Kivelson, M. G. 2007, in Handbook of the Solar–Terrestrial Environment, ed. Y. Kamide & A. C.-L. Chian (Berlin: Springer), 470
Koga, D., Chian, A. C.-L., Miranda, R. A., & Rempel, E. L. 2007, Phys. Rev. E, 75, 046401
Leamon, R. J., Smith, C. W., & Ness, N. F. 1998, Geophys. Res. Lett., 25, 2505
Li, G. 2008, ApJ, 672, L65
Liu, R., Lee, J., Wang, T., Stenborg, G., Liu, C., & Wang, H. 2010, ApJ, 723, L28
Liu, Y., Richardson, D., Belcher, J. W., Kasper, J. C., & Elliott, H. A. 2006, J. Geophys. Res., 111, A01102
Miranda, R. A., Chian, A. C.-L., Dasso, S., Echer, E., Muñoz, P. R., Trivedi, N. B., Tsurutani, B. T., & Yamada, M. 2010, in IAU Symp. 264, Solar and Stellar Variability: Impact on Earth and Planets, ed. A. G. Kosovichev, A. H. Andrei, & J.-P. Rozelot (Cambridge: Cambridge Univ. Press), 363
Mozer, F. S., Angelopoulos, A., Bonnell, J., Glassmeier, K. H., & McFadden, J. P. 2008, Geophys. Res. Lett., 35, L17S04
Müller, W.-C., & Biskamp, D. 2000, Phys. Rev. Lett., 84, 475
Müller, W.-C., Biskamp, D., & Grappin, R. 2003, Phys. Rev. E, 67, 066302
Muñoz, P. R., Chian, A. C.-L., Miranda, R. A., & Yamada, M. 2010, in IAU Symp. 264, Solar and Stellar Variability: Impact on Earth and Planets, ed. A. G. Kosovichev, A. H. Andrei, & J.-P. Rozelot (Cambridge: Cambridge Univ. Press), 369
Nishida, A. 2007, in Handbook of the Solar–Terrestrial Environment, ed. Y. Kamide & A. C.-L. Chian (Berlin: Springer), 280
Paschmann, G. 2008, Geophys. Res. Lett., 35, L19109
Phan, T. D., et al. 2006, Nature, 439, 175
Politano, H., & Pouquet, A. 1995, Phys. Rev. E, 52, 636
Priest, E. R. 2007, in Handbook of the Solar–Terrestrial Environment, ed. Y. Kamide & A. C.-L. Chian (Berlin: Springer), 56
Retinò, A., Sundkvist, D., Vaivads, A., Mozer, F., André, M., & Owen, C. J. 2007, Nat. Phys., 3, 236
Sahai, R., & Chronopoulos, C. K. 2010, ApJ, 711, L53
Schmidt, J. M., & Cargill, P. J. 2003, J. Geophys. Res., 108, A1023
She, Z.-S., & Leveque, E. 1994, Phys. Rev. Lett., 72, 336
Sonnerup, B. U. O., & Cahill, L. J. 1967, J. Geophys. Res., 72, 171
Sonnerup, B. U. O., et al. 1981, J. Geophys. Res., 86, A10049
Stone, E. C., Cummings, A. C., McDonald, F. B., Heikkila, B. C., Lal, N., & Webber, W. R. 2008, Nature, 454, 71
Veltri, P. 1999, Plasma Phys. Control. Fusion, 41, A787
Vörös, Z., Leubner, M. P., & Baumjohann, W. 2006, J. Geophys. Res., 111, A02102
Wei, F. S., Hu, Q., Feng, X. S., & Fang, Q. 2003a, Space Sci. Rev., 107, 107
Wei, F. S., Liu, R., Fan, Q., & Feng, X. S. 2003b, J. Geophys. Res., 108, A1263
Welch, P. D. 1967, IEEE Trans. Audio Electroacoust., AU-15, 70
Zhou, Y., Matthaeus, W. H., & Dmitruk, P. 2004, Rev. Mod. Phys., 76, 1015
Zuo, P. B., Wei, F. S., Feng, X. S., Xu, X. J., & Song, W. B. 2010, J. Geophys. Res., 115, A10102